Microsatellite marker analysis was performed using the ABI Prism Linkage Mapping Set with D15S1002 and analyzed by GeneMapper (Applied Biosystems, Foster City, CA). In the deletion region of STS, no marker was available for the ABI Prism Linkage Mapping Set. Thus, the single-nucleotide polymorphisms (SNP) typing was carried out. From the STS deletion region of 5q35, eight SNPs, IMS-JST038690, IMS-JST087588, IMS-JST087589, IMS-JST183486, IMS-JST172005, IMS-JST073857, IMS-JST087921, and IMS-JST087922, were selected using in silico library, Japanese Single Nucleotide Polymorphisms (JSNP) database (http://snp.ims.u-tokyo.ac.jp/index.html). Allelic types were analyzed by PCR-direct sequencing method using the BigDye terminator (Applied Biosystems, Foster City, CA).

RESULTS

By aCGH analysis, loss of the genomic copy numbers was identified in the region of 15q11.2, which is responsible and typical for PWS (Fig. 3A). The concurrent deletion was
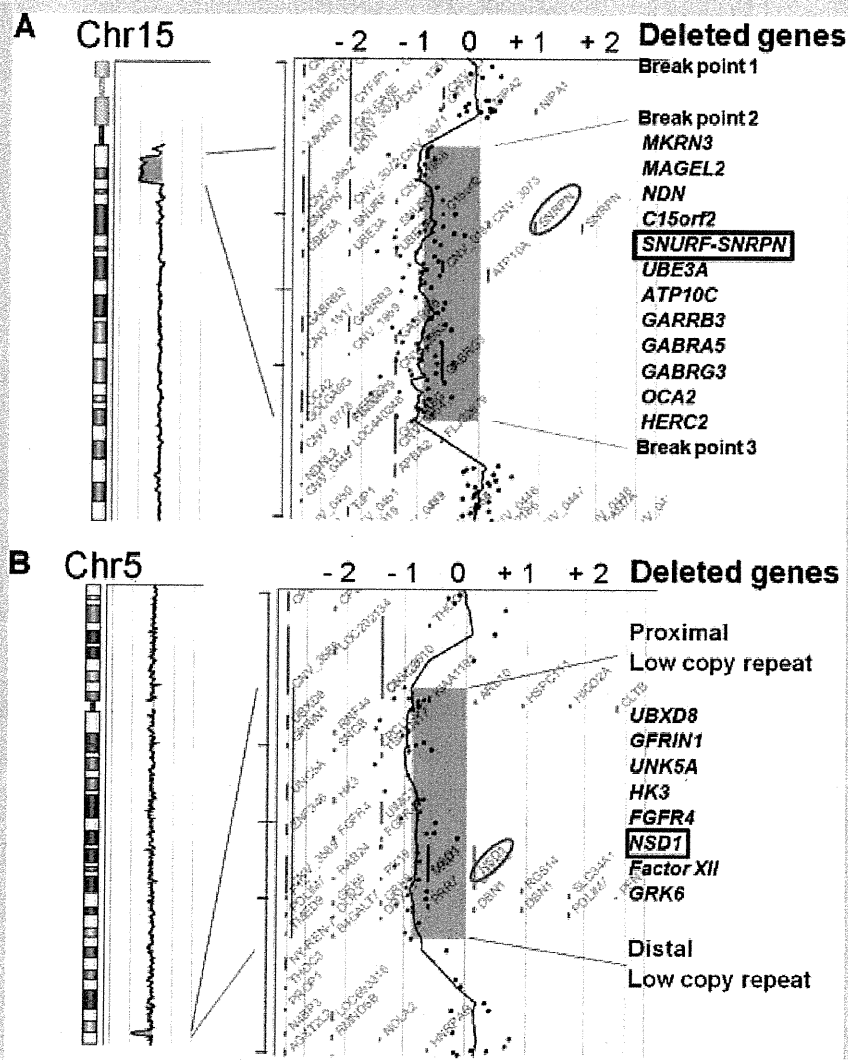

FIG. 3. aCGH profiles of the patient shown by CGH Analytics in Chromosome view (left) and Gene view (right). A: Typical deletion of PWS region including *SNRPN* is shown. B: Typical STS deletion including *NSD1* is indicated. The horizontal axis indicates the log 2 ratio of the genomic copy number. The blue rectangles indicate the regions containing copy number aberrations. The aberration areas are expanded in Gene view (right). The dots indicate the locations and the corresponding log 2 ratios of the probes. The red circles emphasize *SNRPN* and *NSD1*.
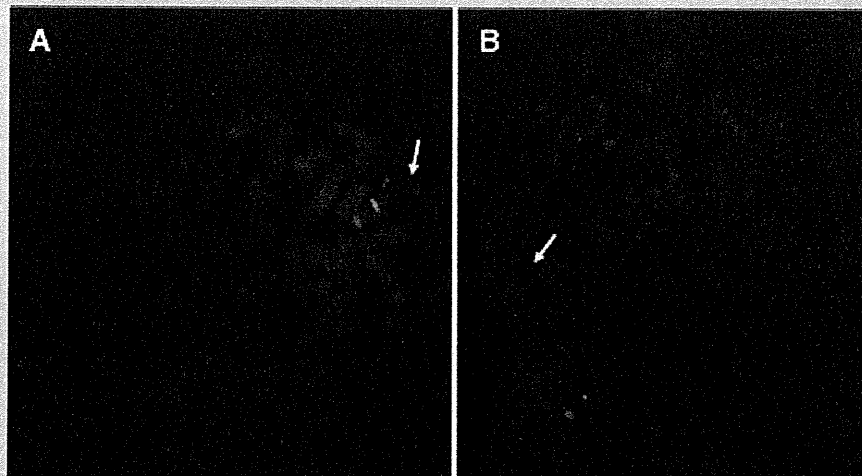
FIG. 4. FISH analysis to confirm the chromosomal deletion. A: One of the green signals covering *SNRPN*, RP11-1071C22 (15q11.2; 22601976–22822028), was deleted. Two red signals are the markers of chr15, RP11-48A4 (15q26.3; 99433829–99587322). B: One of the green signals covering *NSD1*, RP11-99N22 (5q35.2–5q35.3; 176474586–176655375), was deleted, whereas two red labeled RP11-94J21 (5p15.33; 1377471–1540913) signals were confirmed in all cells. Physical positions are referred to NCBI Build 36.1. White arrows indicate abnormal chromosomes in each FISH image.

identified in the region of 5q35, which is also responsible and typical for STS (Fig. 3B). FISH analyses confirmed the deletion of both regions (Fig. 4). There were no deletions of PWS region and STS region in both parents indicating de novo occurrence (data not shown).

To confirm the parental origin of both deletions, polymorphic markers were analyzed in the patient and his parents. Regarding the 15q11.2 region, the patient showed an only allele with 112-bp common to his mother, indicating the deletion of paternal allele (Fig. 5A). Among eight analyzed SNPs, only IMS-JST183486 was informative. The patient showed hemizyogous of T at the SNP position, whereas the father and the mother showed homozygous of A and T, respectively (Fig. 5B). From the result, we concluded that both deletions were derived from the paternal allele.

DISCUSSION

Initially, the patient was diagnosed as PWS due to severe hypotonia, hypopigmentation, hypoplastic genitalia, and small hands and feet. It was supported by hyperphagia and obesity which later developed. However, his facial features including relative macrocephaly, protruding forehead, frontal baldness, strabismus, downslanting palpebral fissures, and pointed chin were atypical for PWS. He also showed congenital cardiac anomalies, hydronephrosis, and epilepsy, which are rare findings in PWS. Severe hypotonia and severe developmental delay were also atypical for PWS. This was the reason why we analyzed genomic copy numbers.

To the best of our knowledge, this is the first report of co-occurrence of PWS and STS. Translocation between chromosomes 5 and 15 was excluded by G-banded analysis. Array CGH demonstrated that the sizes and locations of the two deletions were typical for both syndromes. Both of the deletions were derived from the paternal chromosome. We suspect that co-occurrence of two deletions is incidental.

His growth curve showed an interesting pattern. He showed overgrowth in the infantile period. Gradually, his growth velocity decreased. Now he shows severe growth deficiency. Although we understand that haploinsufficiency of *NSD1* might lead to height gain and patients with STS show advanced bone age, his growth deficiency was worse compared with standard PWS patients and his bone age was delayed [Nagai et al., 2000]. Growth hormone deficiency and severe scoliosis may explain his growth deficiency. We posit that each deletion contributed independently to the features. Severe growth and developmental delay might be explained by the combined effects of PWS and STS.

There are some reports of concurrent chromosomal aberrations in the same patients [Shimojima et al., 2009]. The result of this study indicates that there may be more frequent co-occurrences of two more deletions than what we think. When a patient shows atypical or overlapping features regardless of a previously established diagnosis, we would recommend investigation of whole genomic copy numbers by aCGH.
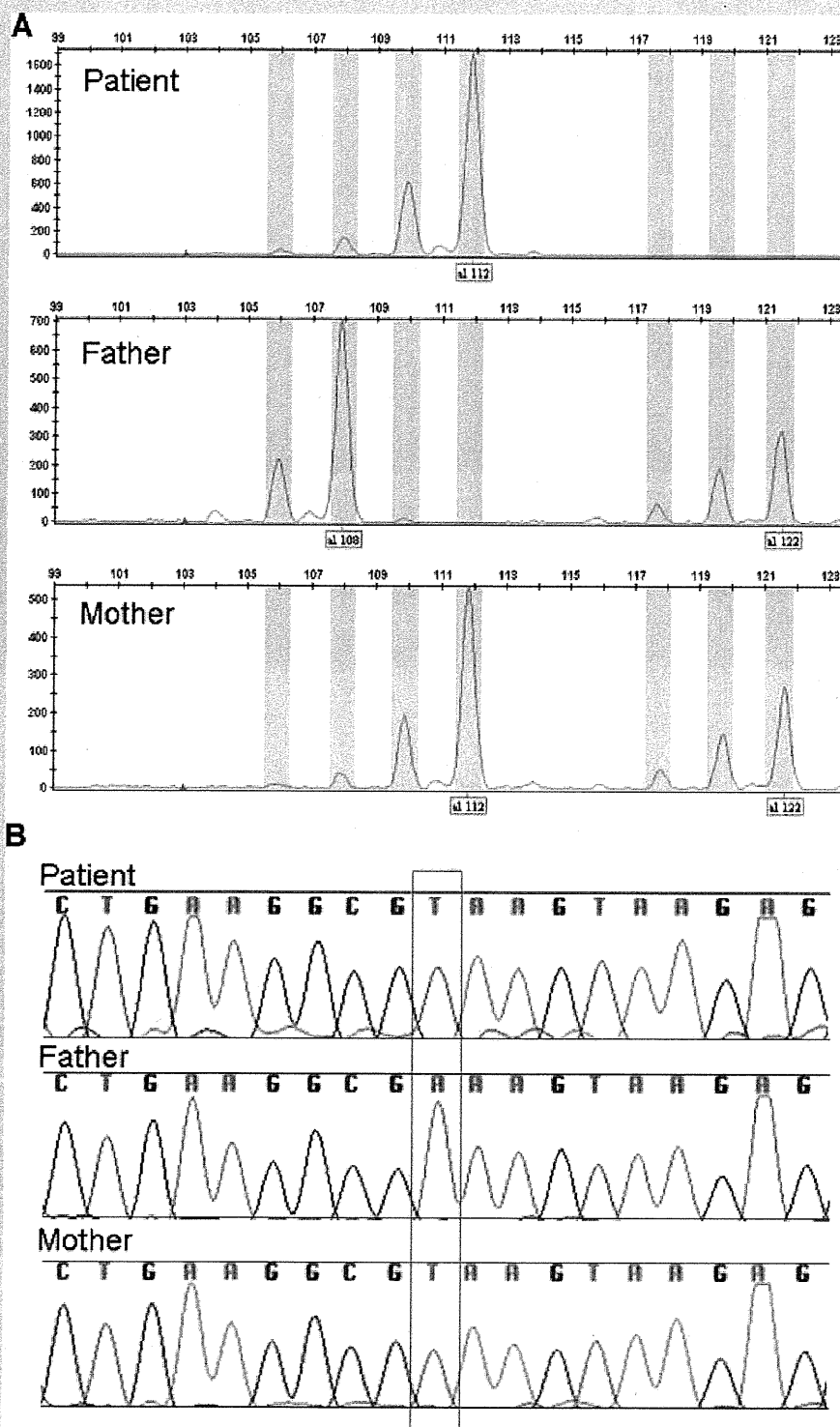
FIG. 5. Molecular analysis of the patient's family. A: GeneMapper analysis using D15S1002. The patient shows only one allele with 112-bp common with his mother, indicating the paternal deletion. B: SNPs analysis of IMS-JST183486. The patient's SNP type as T is only common with his mother, indicating the deletion of paternal allele.

REFERENCES

Holm VA, Cassidy SB, Butler MG. 1993. Prader–Willi syndrome: Consensus diagnostic criteria. Pediatrics 91:398–402.

Kurotaki N, Imaizumi K, Harada N, Masuno M, Kondoh T, Nagai T, Ohashi H, Naritomi K, Tsukahara M, Makita Y, Sugimoto T, Sonoda T, Hasegawa T, Chinen Y, Tomita Ha HA, Kinoshita A, Mizuguchi A, Yoshiura T, Ki K, Ohta T, Kishino T, Fukushima Y, Niikawa N, Matsumoto N. 2002. Haploinsufficiency of NSD1 causes Sotos syndrome. Nat Genet 30:365–366.

Kurotaki N, Stankiewicz P, Wakui K, Niikawa N, Lupski JR. 2005. Sotos syndrome common deletion is mediated by directly oriented subunits within inverted Sos-REP low-copy repeats. Hum Mol Genet 14:535–542.

Ledbetter DH, Riccardi VM, Airhart SD. 1981. Deletion of chromosome 15 as a cause of Prader–Willi syndrome. N Engl J Med 304:325–329.

Miyake N, Kurotaki N, Sugawara H, Shimokawa O, Harada N, Kondoh T, Tsukahara M, Ishikiriyama S, Sonoda T, Miyoshi Y, Sakazume S, Fukushima Y, Ohashi H, Nagai T, Kawame H, Kurosawa K, Touyama M, Shiihara T, Okamoto N, Nishimoto J, Yoshiura K, Ohta T, Kishino T, Niikawa N, Matsumoto N. 2003. Preferential paternal origin of microdeletions caused by prezygotic chromosome or chromatid rearrangements in Sotos syndrome. Am J Hum Genet 72:1331–1337.

Nagai T, Matsuo N, Kayanuma Y, Tonoki H, Fukushima Y, Ohashi H, Murai T, Hasegawa T, Kuroki Y, Niikawa N. 2000. Standard growth curves for Japanese patients with Prader–Willi syndrome. Am J Med Genet 95:130–134.

Nagai T, Matsumoto N, Kurotaki N, Harada N, Niikawa N, Ogata T, Imaizumi K, Kurosawa K, Kondoh T, Ohashi H, Tsukahara M, Makita Y, Sugimoto T, Sonoda T, Yokoyama T, Uetake K, Sakazume S, Fukushima Y, Naritomi K. 2003. Sotos syndrome and haploinsufficiency of NSD1: Clinical features of intragenic mutations and submicroscopic deletions. J Med Genet 40:285–289.

Sahoo T, del Gaudio D, German JR, Shinawi M, Peters SU, Person RE, Garnica A, Cheung SW, Beaudet AL. 2008. Prader–Willi phenotype caused by paternal deficiency for the HBII-85 C/D box small nucleolar RNA cluster. Nat Genet 40:719–721.

Shimojima K, Páez MT, Kurosawa K, Yamamoto T. 2009. Proximal interstitial 1p36 deletion syndrome: The most proximal 3.5-Mb microdeletion identified on a dysmorphic and mentally retarded patient with inv(3)(p14.1q26.2). Brain Dev 31:629–633.

Visser R, Shimokawa O, Harada N, Kinoshita A, Ohta T, Niikawa N, Matsumoto N. 2005. Identification of a 3.0-kb major recombination hotspot in patients with Sotos syndrome who carry a common 1.9-Mb microdeletion. Am J Hum Genet 76:52–67.

Original Article

Four mood stabilizers commonly induce FEZ1 expression in human astrocytes

Yu Z, Ono C, Kim HB, Komatsu H, Tanabe Y, Sakae N, Nakayama KI, Matsuoka H, Sora I, Bunney WE, Tomita H. Four mood stabilizers commonly induce FEZ1 expression in human astrocytes.
Bipolar Disord 2011: 13: 486–499. © 2011 The Authors.
Journal compilation © 2011 John Wiley & Sons A/S.

Objectives: Mood stabilizers influence the morphology, chemotaxis, and survival of neurons, which are considered to be related to the mood-stabilizing effects of these drugs. Although previous studies suggest glial abnormalities in patients with bipolar disorder and an effect of mood stabilizers on certain genes in astrocytes, less is known about the effects of mood stabilizers in astrocytes than in neurons. The present study identifies a common underlying response to mood stabilizers in astrocytes.

Methods: Human astrocyte-derived cells (U-87 MG) were treated with the four most commonly used mood stabilizers (lithium, valproic acid, carbamazepine, and lamotrigine) and subjected to microarray gene expression analyses. The most prominently regulated genes were validated by qRT-PCR and western blot analysis. The intercellular localization of one of these regulated genes, fasciculation and elongation protein zeta 1 (FEZ1), was evaluated by immunofluorescence staining.

Results: The microarray data indicated that FEZ1 was the only gene commonly induced by the four mood stabilizers in human astrocyte-derived cells. An independent experiment confirmed astrocytic FEZ1 induction at both the transcript and protein levels following mood stabilizer treatments. FEZ1 localized to the cytoplasm of transformed and primary astrocytes from the human adult brain.

Conclusions: Our data suggest that FEZ1 may play important roles in human astrocytes, and that mood stabilizers might exert their cytoprotective and mood-stabilizing effects by inducing FEZ1 expression in astrocytes.

Zhiqian Yu[a], Chiaki Ono[a], Helen B Kim[b], Hiroshi Komatsu[a,c], Yoichiro Tanabe[a,c], Nobutaka Sakae[d], Keiichi I Nakayama[e], Hiroo Matsuoka[c], Ichiro Sora[a], William E Bunney[b] and Hiroaki Tomita[a]

[a]Department of Biological Psychiatry, Tohoku University Graduate School of Medicine, Sendai, Japan, [b]Department of Psychiatry and Human Behavior, University of California, Irvine, Irvine, CA, USA, [c]Department of Psychiatry, Tohoku University Graduate School of Medicine, Sendai, [d]Department of Neurology, Neurological Institute, [e]Department of Molecular and Cellular Biology, Medical Institute of Bioregulation, Kyushu University, Fukuoka, Japan

Corresponding author:
Hiroaki Tomita, M.D., Ph.D.
Department of Biological Psychiatry
Tohoku University Graduate School of Medicine
2-1 Seiryo-machi, Aoba-ku
Sendai, 980-8575, Japan
Fax: 81-22-717-7809
E-mail: htomita@med.tohoku.ac.jp

Mood stabilizers, such as lithium (Li), valproic acid (VPA), carbamazepine (CBZ), and lamotrigine (LTG), are effective in ameliorating manic and depressive symptoms and in preventing the relapse and recurrence of bipolar disorder (BD). Mood stabilizers have significant effects on the cell survival, morphology, and chemotaxis of neuronal cells, and the neuroprotective effects of mood stabilizers are considered to be related to

---

The authors of this paper do not have any commercial associations that might pose a conflict of interest in connection with this manuscript.

the mood-stabilizing effects of the drugs (1). For example, Li, VPA, and CBZ inhibit growth cone collapse and increase the spread area of growth cones (2). Various molecules, such as β-arrestin 2, glycogen synthase kinase-3 and phosphatidylinositol signaling pathways, and histone deacetylases, have been suggested as candidate targets of mood stabilizers (3–7). Evidence also suggests that the drugs exert mood-stabilizing and neuroprotective effects by altering the transcriptional regulation of various genes in the brain, including B-cell lymphoma 2 (BCL2) and ionotropic glutamate receptors type AMPA 1 (GRIA1) and type

AMPA 2 (GRIA2) (8, 9), potentially as downstream effectors of the target molecules of mood stabilizers.

Since these previous studies investigating the molecular mechanisms of mood stabilizers focused primarily on neuronal cells and used either neuronal cells or brain tissues, which are heterogeneous mixtures of various types of neuronal, glial, and vascular cells, the biological effects of mood stabilizers on astrocytes remain largely unknown. Since the function of astrocytes includes regulation of the extracellular concentrations of ion and neurotransmitters, modification of synaptic efficacy, maintenance of the blood-brain barrier, and structural as well as trophic support of neurons and oligodendrocytes (10–14), it is reasonable to expect that mood stabilizers may exert at least part of their mood-stabilizing and neuroprotective effects by affecting these astrocytic functions. Indeed, some studies suggest the potential involvement of astrocytes in the pathogenesis of BD. Many postmortem brain studies of patients with BD have demonstrated abnormalities in the density and shape of glial cells, as well as decreased levels of the astrocyte marker, glial fibrillary acidic protein (GFAP) (15). Glia are markedly reduced in the subgenual prefrontal cortex of patients with BD, and this reduction is most prominent in patients with familial BD (16). Mean glial density is significantly reduced in sublayers IIIc and Vb of the prefrontal cortex in patients with BD, whereas the mean size of glial cell bodies is increased in layers I and IIIc, which can be attributed to the increased density of extra-large glia in those layers (17). Although previous studies have also shown that the density and size of cortical neurons are reduced in mood disorders, these neuronal reductions are more subtle compared to the glial alterations (18). Furthermore, astrocyte-specific GFAP transcripts are significantly decreased in white matter, and tend to be decreased in gray matter of the anterior cingulate cortex of patients with BD (19). The decrease in GFAP expression was confirmed in a proteomic study of the frontal cortex of patients with BD (20). S100B, which is produced and secreted by astrocytes, is significantly increased in the serum of patients during episodes of manic and depressive states (21). S100B exerts trophic and/or toxic effects on neuronal and glial cells depending on its concentration and has been reported to be a susceptibility gene for a subgroup of BD patients presenting with psychotic symptoms (22). Thus, while current evidence is not conclusive, it does seem to suggest that a dysfunction or a loss of astrocytes may at least in part underlie the pathogenesis of BD.

Moreover, several studies have shown that mood stabilizers exert biological effects on astrocytes. Li has been shown to suppress the extracellular signal-regulated protein kinase pathway (23), whereas VPA increases the expression of neurotrophic factors in astrocytes (24). Li, VPA, and CBZ decrease myo-inositol uptake activity (25) and kainate receptor subunit GluR6 (GRIK2) expression in astrocytes (26), whereas Li, VPA, and CBZ increase the pH and cytosolic phospholipase A2 (cPLA2) levels in astrocytes (27, 28). It is worth noting that while these mood stabilizers have distinct chemical characteristics, they affect common molecular and cellular pathways in astrocytes.

Taken together, these studies suggest glial abnormalities in patients with BD and an effect of mood stabilizers on certain genes in astrocytes. However, the effects of mood stabilizers on astrocytes have been much less characterized compared to their effects on neuronal cells. To identify the most prominent biological effect of mood stabilizers on human astrocytes, we conducted microarray-based comprehensive gene expression analyses of a human astrocyte cell line treated with four major mood stabilizers, Li, VPA, CBZ, and LTG, and corresponding controls. We found a transcriptional regulation that was unique to each mood stabilizer and common molecules that were regulated by all four mood stabilizers. Fasciculation and elongation protein zeta 1 (FEZ1) was the only gene that was upregulated by all four mood stabilizers at both the mRNA and the protein expression levels. This finding points to FEZ1 as a candidate gene involved in the mechanism responsible for the mood-stabilizing effect of the tested drugs.

Materials and methods

Cell lines and cultures

The astrocyte-derived human cell line U-87 MG and the neuron-derived human cell line SK-N-SH were purchased from the American Type Culture Collection. The human oligodendroglioma cell line (OL) was a gift from Dr. Juan Carlos De La Torre from the Scripps Research Institute, La Jolla, CA, USA. Primary astrocytes from the human brain cortex (ACBRI 371) were purchased from Applied Cell Biology Research Institute, Kirkland, WA, USA. For the microarray studies, U-87 MG cells (6×10^8 cells) were suspended in 30 ml of Modified Eagle's Medium [(MEM) Sigma-Aldrich, St. Louis, MO, USA] containing 10% inactive fetal bovine serum (Biological Industries, Beit-Haemek, Israel) and divided into six plastic T75 cell culture flasks (Nalge Nunc Int., Rochester, NY, USA). Li (Kanto

487

Chemical, Tokyo, Japan) and VPA (Sigma-Aldrich) were dissolved directly in MEM at therapeutic concentrations of 0.75 mM and 0.5 mM, respectively. Cells cultured in non-treated (drug-free) MEM were used as controls to evaluate the effects of Li and VPA. The water-insoluble agents CBZ (Sigma-Aldrich) and LTG (Sigma-Aldrich) were dissolved in 100% dimethyl sulfoxide (DMSO) at 33.3 mM and 3.33 mM, respectively (666.6 times the final concentrations) and then resuspended into MEM at 50 μM and 5 μM, respectively, each of which is within the therapeutic range. Since the final DMSO concentration of CBZ- and LTG-containing MEM was 0.15%, control cells were cultured in MEM containing 0.15% DMSO. U-87 MG cells were evenly split into six flasks in MEM and maintained at 37°C in a humidified atmosphere containing 5% CO_2 for 18 hours. The media were replaced with MEM which included Li-, VPA-, CBZ-, LTG-, DMSO-containing, or non-treated MEM and cultured in the same chamber for five days. After a week of exposure to each condition, the media were removed from each flask, and the cells were washed and collected in phosphate buffered saline. To distinguish the biological effects of the mood stabilizers from artifacts, all of the experimental procedures were replicated following completion of the first set of experiments, and two sets of six types of cultured cells were subjected to the following microarray experiments. To validate the microarray expression data by quantitative real-time PCR (qRT-PCR), U-87 MG cells (1×10^8 cells) were cultured in the six different media in the presence or absence of mood stabilizers for five days, in the same manner as in the microarray experiment. For each conditioned medium, the cell culture was replicated in six independent T75 flasks (in total, 6 types of media $\times$ 6 replicates = 36 samples). To evaluate the effect of high-dose mood stabilizer treatments on protein levels by western blot, cells were cultured for five days with higher concentrations (near the maximum limit of the therapeutic ranges) of Li, VPA, CBZ, or LTG (1.2 mM, 1 mM, 100 μM, and 50 μM, respectively). Given the limited quantity of ACBRI371 cells, U-87 MG cells were used for microarray and qRT-PCR analyses, while ACBRI371 cells were used only to determine FEZ1 localization by immunocytochemistry.

RNA extraction and microarray experiments

Total RNA was extracted, DNase-digested, and purified using the RNeasy Mini Kit, RNase-free DNase I, and the RNeasy MinElute Cleanup Kit (Qiagen, Valencia, CA, USA). The RNA integrity number (RIN) for each RNA sample was confirmed to be > 9.8 using the Agilent 2100 Bioanalyzer (Agilent, Santa Clara, CA, USA), and the ribosomal RNA S28/S18 ratio was > 1.9. From the 12 total RNA samples, biotinylated cRNA were synthesized and applied to Illumina BeadChips according to the manufacturer's directions. In brief, biotinylated cRNA was prepared from 500 ng of total RNA using the Illumina Ambion RNA Amplification Kit (Ambion, Austin, TX, USA). The biotinylated cRNA samples were hybridized to Illumina Human-6v2 Expression BeadChips (Illumina, San Diego, CA, USA). Each BeadChip was washed and scanned with Illumina Bead Station 500X.

Data analysis and selection criteria for mood-stabilizer-regulated genes

The inter-array variation among 12 BeadChip microarrays (for 6 types of media $\times$ experimental duplication) was normalized using average normalization after subtracting the background signal intensities. The probability of observing a certain signal intensity level for a set of beads lacking specific probe-target hybridization was calculated as the detection p-value for each probe. The above procedure was performed using Illumina BeadStudio 3.1 software (Illumina). Among the 48,701 transcripts designed on the BeadChip, 11,214 transcripts with signal intensities > 20 and with detection p-values of < 0.05 in all of the 12 U-87 MG samples were considered reliably detectable, and the signal intensities of these transcripts in Li- and VPA-treated cells and in non-treated cells were compared. The signal intensities in CBZ- and LTG-treated cells and in DMSO-treated cells were also compared. Transcripts with consistent fold changes of > 1.2 or < 0.833 in both experimental duplicates were defined as *mood-stabilizer-induced* or *mood-stabilizer-suppressed* genes, respectively. Changes in mRNA expression are consistent among duplicated microarrays when altered genes are selected with a cut-off fold change of > 1.2 or < 0.833, criteria widely used in microarray analyses (29–31). The probability of observed number of overlapping genes in proportion to the expected number was calculated based on hypergeometric distribution, and a p-value of < 0.05 was considered statistically significant. Assuming that among the 48,701 probes, the number of genes altered by drugs A and B are 'a' and 'b' respectively, and effects of treatments are irrelevant, the expected number of overlapping genes between the lists of genes altered by drugs A and B is (a $\times$ b)/48,701.

Hierarchical clustering

To evaluate similarities between the effects of mood stabilizers on expression profiles, the fold change values for the signal intensities of mood-stabilizer-treated samples, relative to the signal intensities determined for the control samples (Li/non-treated control, VPA/non-treated control, CBZ/DMSO-treated control, LTG/DMSO-treated control), were log2 transformed and subjected to an average linkage hierarchical clustering analysis using Genesis software 1.7.5 (available at http://www.genome.tugraz.at). To minimize the confounding effect of DMSO added to CBZ, LTG, and the corresponding control samples, 1,306 genes differentially expressed between the non-treated and DMSO-treated control samples with a fold change of > 1.2 or < 0.833 in at least one of the duplicated experiments were eliminated from the analyses. Among the 11,214 reliably detectable transcripts (with signal intensities > 20 and with detection p-values < 0.05 in all 12 U-87 MG samples), 9,908 transcripts, levels of which were similar between DMSO-treated and untreated samples, were subjected to hierarchical clustering analysis.

Quantitative real-time PCR experiments

Total RNA was extracted from the 36 cell samples [6 types of media (Li, VPA, CBZ, LTG, DMSO-treated control, non-treated control) × 6 replicates] in the same manner employed for the microarray experiment and subjected to cDNA synthesis with random primers using the SuperScript VILO cDNA synthesis kit (Invitrogen, Carlsbad, CA, USA). The relative copy number of each transcript in each cDNA sample was measured using specific primers and iQ SYBR Green Supermix (Bio-Rad, Hercules, CA, USA) with a CFX96 real-time PCR detection system (Bio-Rad). The PCR cycling parameters were as follows: 3 min at 95°C, followed by 40 cycles of 10 sec at 95°C and 30 sec at the annealing temperatures of 55°C to 65°C suitable for each primer set. The target genes were selected based on the microarray data and β-actin (ACTB) was used as an internal control for normalization. The forward and reverse primers for FEZ1 were 5'-GGGACTGCATGAGAC CATGT-3' and 5'-TTGAGGGCTGTAGCCAG ACT-3', respectively. The forward and reverse primers for RNA binding motif protein 14 (RBM14) were 5'-GCAAAGAAGTGAAGGG CAAG-3' and 5'-AAAGCCTGCTGGTAGTC GAA-3', respectively. The forward and reverse primers for ACTB were 5'-CACACTGTGCC

CATCTACGA-3' and 5'-CCATCTCTTGCTC GAAGTCC-3', respectively. Threshold cycles were measured for triplicate samples. A standard curve was constructed for each assay to adjust for differences in the amplification efficiency between primer sets. Differences in the abundance of target genes relative to ACTB among Li-treated samples (n = 6), VPA-treated samples (n = 6) and their non-treated controls (n = 6) were evaluated by one-way analysis of variance (ANOVA) followed by the Dunnett post-hoc test. Likewise, differences in target gene expression levels among CBZ-treated samples (n = 6), LTG-treated samples (n = 6), and their DMSO-treated controls (n = 6) were evaluated by ANOVA.

Western blotting

U-87 MG cells treated with mood stabilizers and control samples were homogenized in phosphate buffered saline (PBS) containing Triton X-100, 4-(2-hydroxyethyl)-1-piperazineethanesulfonic acid (HEPES), bovine serum albumin, gentamicin sulfate, and a proteinase inhibitor cocktail containing 4-(2-aminoethyl) benzenesulfonyl fluoride, aprotinin, leupeptin, bestatin, and pepstatin A (all from Sigma-Aldrich). The supernatant obtained after centrifugation (10,000 × g for 10 min at 4°C) was subjected to sodium dodecyl sulfate polyacrylamide gel electrophoresis (SDS-PAGE) and western blotting with the following primary antibodies: polyclonal goat anti-FEZ1 antibody (1:10000; Abcam, Cambridge, UK) and monoclonal mouse anti-ACTB antibody (1:10000; Sigma-Aldrich). The secondary antibodies employed were horseradish peroxidase-conjugated anti-goat IgG (1:2000; Dako, Glostrup, Denmark) and anti-mouse IgG (1:5000; Jackson ImmunoResearch, West Grove, PA, USA), respectively. Chemiluminescence was detected using an Amersham ECL Plus western blotting detection kit (GE Healthcare, Waukesha, WI, USA) and a LAS-1000 luminescence image analyzer (Fujifilm, Tokyo, Japan), and the results were quantified using ImageJ 1.42 software (http://rsb.info.nih.gov/ij/).

Immunostaining

FEZ1 protein has been shown to be preferentially expressed in neurons but not in astrocytes or oligodendrocytes in the rat brain (32). However, the expression of FEZ1 protein in human brain-derived cells has not been investigated. To determine the expression of FEZ1 proteins in human brain astrocyte cells (U-87 MG and ACBRI 371), neurons (SK-N-SH) and oligodendrocytes (OL)

were placed in a LAB-TEK glass 2-well (1×10^3 cells/well) chamber slide (Nunc, Rochester, NY, USA) together with 1 ml of the appropriate medium (MEM for U-87 MG, ACBRI 371, SK-N-SH; DMEM for OL) and incubated at 37°C, 5% CO_2 for six days. After fixation with ice-cold ethanol/acetone, cells were blocked in PBS containing 1% BSA (Sigma-Aldrich) and 10% normal horse serum (Dako) for 30 min at room temperature. After an overnight incubation at 4°C with primary antibodies, the cells were rinsed in PBS and then incubated at room temperature in the dark with secondary antibody. The primary antibodies used were as follows: polyclonal goat anti-FEZ1 antibody (1:5000; Abcam), polyclonal rabbit anti-GFAP antibody (1:200; Abcam) and monoclonal anti-NeuN antibody (1:200; Abcam). The corresponding secondary antibodies were as follows: Alexa Fluor 488 anti-goat IgG or Alex Fluor 594 anti-rabbit IgG (1:300; Invitrogen). Following incubation with the secondary antibody, the tissues were rinsed in PBS and subjected to nuclear staining with 4, 6-diamidino-2-phenylindole (DAPI) (Invitrogen). Microscopic images were captured using a Leica DAS Mikroskop microscope (Leica Microsystems, Wetzlar, Germany). To evaluate the effects of the four mood stabilizers on FEZ1 localization in U-87 MG cells, cells were cultured for five days with six different treatments (i.e., 1.2 mM Li, 1 mM VPA, 100 µM CBZ, 50 µM LTG, DMSO, and non-treated) in LAB-TEK chamber slides, and subjected to the above-mentioned immunostaining procedure.

Results

Microarray gene expression profiles

Among the 11,214 genes expressed in at least one of the 12 U-87 MG samples treated with or without mood stabilizers (6 types of media × 2 replicates = 12 samples), 65, 797, 315, and 641 genes were found to be induced with a fold change of > 1.2 (20% increase) by the Li, VPA, CBZ, and LTG treatments, respectively. In contrast, 142, 1008, 80, and 543 genes were suppressed with a fold change of < 0.833 (20% decrease) by the mood stabilizer treatments, respectively (Fig. 1). Tables 1 and 2 show gene symbols for the 10 most robustly up- and down-regulated genes in response to each mood stabilizer treatment, some of which have functions relevant to the mechanism of action of each mood stabilizer. VPA and LTG tended to affect more genes at the transcriptional level in astrocyte-derived cells, whereas the cellular effects

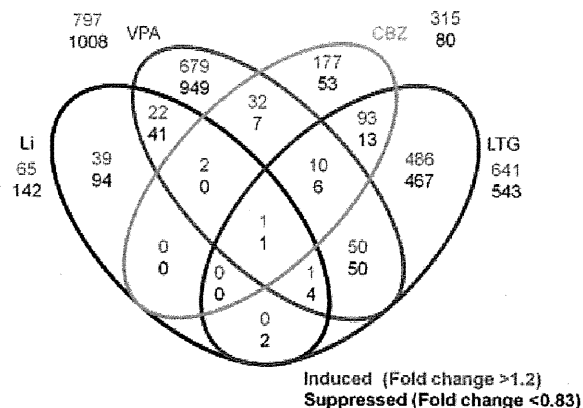Induced (Fold change >1.2)
Suppressed (Fold change <0.83)

Fig. 1. Venn diagram summarizing the number of genes altered by each mood stabilizer and the overlaps among the genes altered by each mood stabilizer. Genes were selected according to the following criteria: a fold change > 1.2 (red) or < 0.83 (black) in both of the duplicated pairs of microarrays, a signal intensity > 20, and a detection p-value < 0.05 in all microarrays. Li = lithium; VPA = valproic acid; CBZ = carbamazepine; LTG = lamotrigine.

of the Li and CBZ treatments at the therapeutic concentrations used were relatively modest. Li and VPA commonly induced 26 genes and suppressed 46 genes, whereas Li demonstrated little overlap with the other anticonvulsants (3 induced genes and 1 suppressed gene in common between Li- and CBZ-treated samples; 2 induced and 7 suppressed genes in common between Li- and LTG-treated samples). The observed number of commonly regulated genes between Li- and VPA-treated samples was significantly higher than the expected number (p < 0.001). Furthermore, the observed number of commonly induced/suppressed genes between CBZ- and LTG-treated samples (104 and 20 genes, respectively) was also significantly higher than the expected number (p < 0.001). Hierarchical clustering analysis of the signal intensity ratio of mood-stabilizer-treated cells divided the four mood stabilizers into two groups, Li-VPA and CBZ-LTG (Fig. 2), which was consistent with the numbers of overlapping genes among the four mood stabilizers.

Induction of FEZ1 expression in human astrocytic cells

FEZ1 was the only gene induced by all four mood stabilizers. The microarray data revealed that the FEZ1 mRNA expression level was increased by 34%, 119%, 35%, and 115% after treatment with Li, VPA, CBZ, and LTG, respectively (Fig. 3A). FEZ1 was the top 5th, 141st, 193rd, and 10th most highly expressed gene among the total genes induced by Li, VPA, CBZ, and LTG, respectively (Table 1).

Table 1. The 10 most induced genes in response to each mood stabilizer

	Lithium			Valproic acid			Carbamazepine			Lamotrigine		
Rank	Symbol	Fold change	Function	Symbol	Fold change	Function	Symbol	Fold change	Function	Symbol	Fold change	Function
1	MMP14	1.40	Proteolysis	TSPAN7	5.05	Glycosylation	KIAA1033	1.91	Uncharacterized	PAIP1	2.00	RNA stabilization
2	RASIP1	1.37	Uncharacterized	CA2	3.55	One-carbon metabolism	NIPBL	1.83	Cell cycle	DNAJC10	1.87	Protein folding
3	C21orf70	1.33	Uncharacterized	LRRN3	3.33	Activation of MAPK activity	PAIP1	1.61	RNA stabilization	TUBG1	1.78	Cytoskeleton organization
4	FABP4	1.32	Proliferation	GABRB1	3.30	Ion channel complex	POLH	1.60	DNA repair	CUTA	1.76	Protein complex assembly
5	FEZ1	1.32	Cell motion/ axon guidance	GAP43	3.28	Cell motion/ axon guidance	AS3MT	1.54	Xenobiotic metabolism	KIAA1033	1.73	Uncharacterized
6	AAMP	1.31	Cell motion	ASAP3	3.20	Small GTPase signaling	ZKSCAN4	1.52	Transcription	MMP1	1.71	Proteolysis
7	LENG8	1.30	Uncharacterized	TNFAIP6	3.02	Cell adhesion	ERMN	1.52	Cytoskeleton organization	DDX59	1.70	Uncharacterized
8	MYCL1	1.30	Regulation of transcription	VGF	2.91	Cell-cell signaling	FAR1	1.50	Fatty acid metabolism	CSNK1A1	1.67	Wnt signaling
9	CRB2	1.30	Sensory perception	BIRC3	2.91	Anti-apoptosis	MAP3K2	1.50	Activation of MAPK activity	UBE4A	1.66	Proteolysis
10	NDUFB1	1.29	Oxidative phosphorylation	SPINK13	2.88	Uncharacterized	KPNA5	1.50	Intracellular protein transport	FEZ1	1.64	Cell motion/ axon guidance

The table shows the 10 most robust fold changes in the signal intensities of the mood-stabilizer-treated samples divided by the appropriate control samples. Each fold change represents the minimal value among the fold changes determined in four comparisons between duplicate mood-stabilizer-treated samples and duplicate control samples. Columns labeled *Function* indicate representative *biological process* categories from the Gene Ontology database (http://www.geneontology.org/) to which each gene belongs.

Table 2. The 10 most suppressed genes in response to each mood stabilizer

Rank	Lithium			Valproic acid			Carbamazepine			Lamotrigine		
	Symbol	Fold change	Function	Symbol	Fold change	Function	Symbol	Fold change	Function	Symbol	Fold change	Function
1	AFMID	0.63	Tryptophan metabolism	CA9	0.22	One-carbon metabolism	RBM14	0.67	Transcription	ABCD1	0.47	Fatty acid metabolism
2	RBM14	0.65	Transcription	ZP1	0.23	Fertilization	PUS1	0.71	RNA processing	NFIC	0.52	Transcription
3	RIMBP3	0.65	Uncharacterized	KCNS1	0.28	Ion transport	CLIP1	0.73	Cell cycle	PPDPF	0.59	Uncharacterized
4	RAPGEFL1	0.66	Small GTPase signaling	CHI3L2	0.31	Polysaccharide metabolism	HSP90AA1	0.74	Protein folding	ATN1	0.61	Cell death
5	SNORD14A	0.68	Uncharacterized	SERP2	0.32	Protein transport	CDK5RAP3	0.75	Cell cycle	SMARCC2	0.61	Chromatin organization
6	SETD7	0.68	Chromatin organization	OLFML3	0.33	Uncharacterized	AKIRIN1	0.76	Uncharacterized	JOSD2	0.61	Uncharacterized
7	P2RY6	0.68	Ion transport	SLC2A1	0.34	Monosaccharide transport	MAP2K3	0.76	Activation of MAPK activity	SOLH	0.61	Proteolysis
8	ZNF200	0.70	Zinc ion binding	TSPAN10	0.35	Uncharacterized	HIST2H2BF	0.77	Chromatin organization	IFITM3	0.63	Immune response
9	DOCK3	0.71	Uncharacterized	ARTN	0.35	Cell proliferation	CPT1B	0.77	Fatty acid metabolism	SLN	0.63	Calcium ion transport
10	COL4A3BP	0.72	Cell morphogenesis	C10orf10	0.35	Uncharacterized	CTSL1	0.77	Proteolysis	AHDC1	0.63	Uncharacterized

The table shows the 10 least robust fold changes in the signal intensities of the mood-stabilizer-treated samples divided by the appropriate control samples. Each fold change represents the maximal value among the fold changes determined in four comparisons between duplicate mood-stabilizer-treated samples and duplicate control samples. Columns labeled *Function* indicate representative *biological process* categories from the Gene Ontology database (http://www.geneontology.org/) to which each gene belongs.
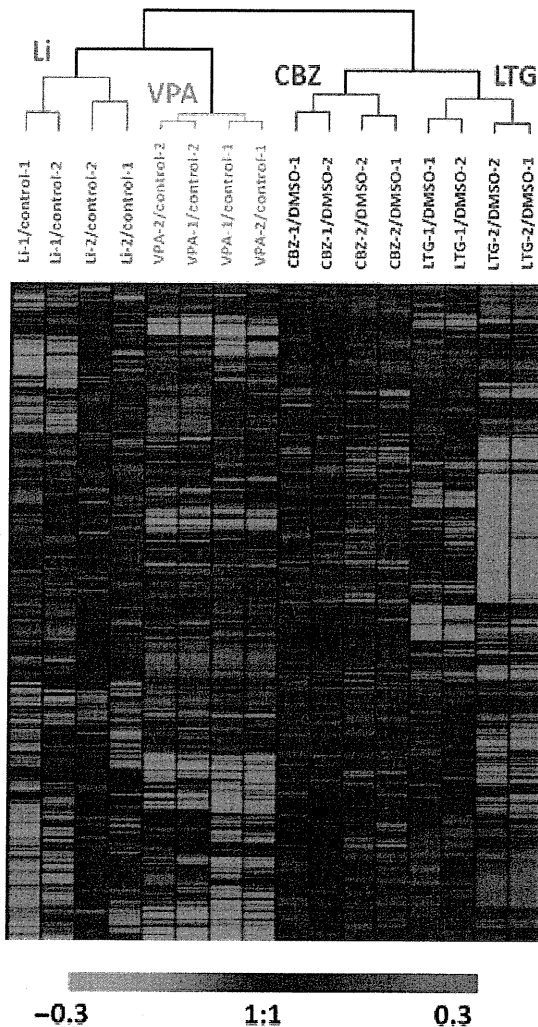
Fig. 2. Hierarchical clustering of gene expression changes caused by the mood stabilizers. Log_2-transformed ratios of the signal intensities of samples treated with mood stabilizers to the signal intensities of their controls [lithium (Li)-treated sample/non-treated control, valproic acid (VPA)-treated sample/non-treated control, carbamazepine (CBZ)-treated sample/DMSO-treated control, lamotrigine (LTG)-treated sample/DMSO-treated control] were subjected to an average linkage hierarchical clustering analysis. Ratios for each of the four combinations of duplicate drug-treated samples to their duplicate control samples were calculated.

Verification by qRT-PCR using six independent cell cultures for each mood stabilizer treatment and for the control samples showed that the FEZ1 mRNA levels were significantly increased by 49% ($p < 0.05$), 78% ($p < 0.001$), 42% ($p < 0.01$), and 47% ($p < 0.001$) following treatment with Li (0.75 mM), VPA (0.5 mM), CBZ (50 µM), and LTG (5 µM) (Fig. 3A), respectively. Western blotting analysis demonstrated that the VPA and LTG treatments significantly induced FEZ1 protein expression levels by 36% ($p < 0.05$) and 60%

($p < 0.01$), respectively, at the lower concentrations (0.5 mM and 5 µM, respectively) (Fig. 3B), while neither Li nor CBZ treatment significantly altered FEZ1 protein expression levels at lower concentrations (0.75 mM and 50 µM, respectively). On the other hand, FEZ1 protein expression levels were significantly increased by 42% ($p < 0.05$), 58% ($p < 0.05$), 75% ($p < 0.01$), and 62% ($p < 0.01$) following treatment with the higher concentrations of Li (1.2 mM), VPA (1 mM), CBZ (100 µM), and LTG (50 µM), respectively (Fig. 3C).

Suppression of RBM14 expression in human astrocytic cells

RBM14 was the only gene suppressed by all four mood stabilizers. The microarray data showed that RBM14 was decreased by 39%, 65%, 33%, and 54% following treatment with Li, VPA, CBZ, and LTG, respectively (Fig. 3D). RBM14 was the top 2nd, 808th, 1st, and 146th most robustly downregulated gene among the total genes suppressed by Li, VPA, CBZ, and LTG, respectively (Table 2). qRT-PCR analysis revealed that the mRNA levels of RBM14 were decreased by 37% ($p < 0.001$), 47% ($p < 0.05$), 32% ($p < 0.05$), and 36% ($p < 0.05$) following treatment with Li, VPA, CBZ, and LTG, respectively (Fig. 3D). However, the protein expression levels of RBM14 were not altered in response to any of the mood stabilizer treatments at any of the tested doses (Fig. 3E).

Intracellular localization of FEZ1 in human brain-derived cells

To assess FEZ1 protein expression in human brain-derived cells, the human astrocyte-derived cell line U-87 MG, the human primary astrocyte cells ACBRI 371, the human neuron-derived cell line SK-N-SH, and the human oligodendrocyte-derived cell line OL, the cultures were subjected to immunofluorescent staining with anti-FEZ1 antibody (red) and anti-GFAP (green) or anti-NeuN (green) antibodies. The cell nuclei were stained with 4', 6-diamidino-2-phenylindole (DAPI, blue) and observed under UV excitation. The immunostaining images revealed FEZ1 protein expression in the U-87 MG (Figs. 4A–C), ACBRI 371 (Figs. 4D–F), and SK-N-SH (Figs. 4G–I) cells, but not in OL cells (data not shown). The FEZ1 immunostaining signal was localized in the cytoplasm of human astrocyte- and neuron-derived cells, while the nuclei were immunonegative (arrowheads). There were no differences in intracellular FEZ1 localization in U-87 MG cells after five days of treatment with Li, VPA, CBZ, and LTG (data not shown).
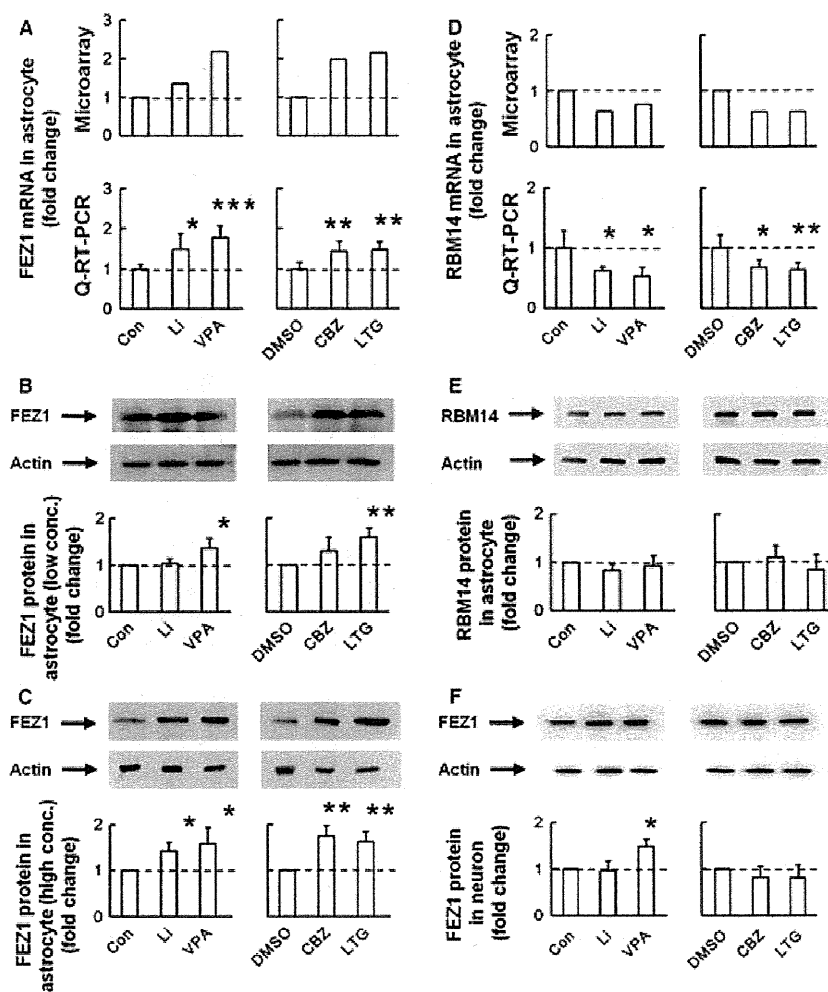
Fig. 3. Transcriptional and protein expression levels of fasciculation and elongation protein zeta 1 (FEZ1) and RNA binding motif protein 14 (RBM14) in astrocytic and neuronal cells after the mood stabilizer treatments. (A) The upper bar graph shows the FEZ1 transcript signal intensities determined from microarray analyses of human astrocyte-derived cells, relative to the averaged signal intensity of the control samples. The lower bar graph shows the FEZ1 transcript levels in human astrocyte-derived cells relative to the averaged signal intensity of the control samples, as measured by qRT-PCR analysis. (B) Gel images and bar graph of the signal intensities determined by western blotting of human astrocyte-derived cells using anti-FEZ1 antibody, after treatment with the lower concentrations of the four mood stabilizers [0.75 mM lithium (Li), 0.5 mM valproic acid (VPA), 50 μM carbamazepine (CBZ), and 5 μM lamotrigine (LTG)], relative to the averaged signal intensity of the control samples. (C) Gel images and bar graph of the signal intensities determined by western blotting of human astrocyte-derived cells using anti-FEZ1 antibody, after treatment with the higher concentrations of the four mood stabilizers (1.2 mM Li, 1 mM VPA, 100 μM CBZ, and 50 μM LTG), relative to the averaged signal intensity of the control samples. (D) The upper bar graph shows the signal intensities for the RBM14 transcript from microarray analyses of human astrocyte-derived cells relative to the averaged signal intensity of the control samples. The lower bar graph shows the transcript levels of RBM14 in human astrocyte-derived cells relative to the averaged signal intensity of the control samples, as measured by qRT-PCR analysis. (E) Gel images and bar graph of the signal intensities determined by western blotting of human astrocyte-derived cells using anti-RBM14 antibody, after treatment with the higher concentrations of the four mood stabilizers (1.2 mM Li, 1 mM VPA, 100 μM CBZ, and 50 μM LTG), relative to the averaged signal intensity of the control samples. (F) Gel images and bar graph of the signal intensities determined by western blotting of human neuron-derived cells using anti-FEZ1 antibody, after treatment with the higher concentrations of the four mood stabilizers (1.2 mM Li, 1 mM VPA, 100 μM CBZ, and 50 μM LTG), relative to the averaged signal intensity of the control samples. Con = non-treated control; DMSO = dimethyl sulfoxide-treated control. $*p < 0.05$; $**p < 0.01$; $***p < 0.001$.

Effect of mood stabilizers on FEZ1 expression in human neuronal cells

To determine whether any of the mood stabilizers affected FEZ1 protein expression levels in human

neuron-derived cells, human neuron-derived SK-N-SH cells were subjected to mood stabilizer treatments in the same manner employed for the U-87 MG experiments. Treatments with any of the four mood stabilizers at the lower
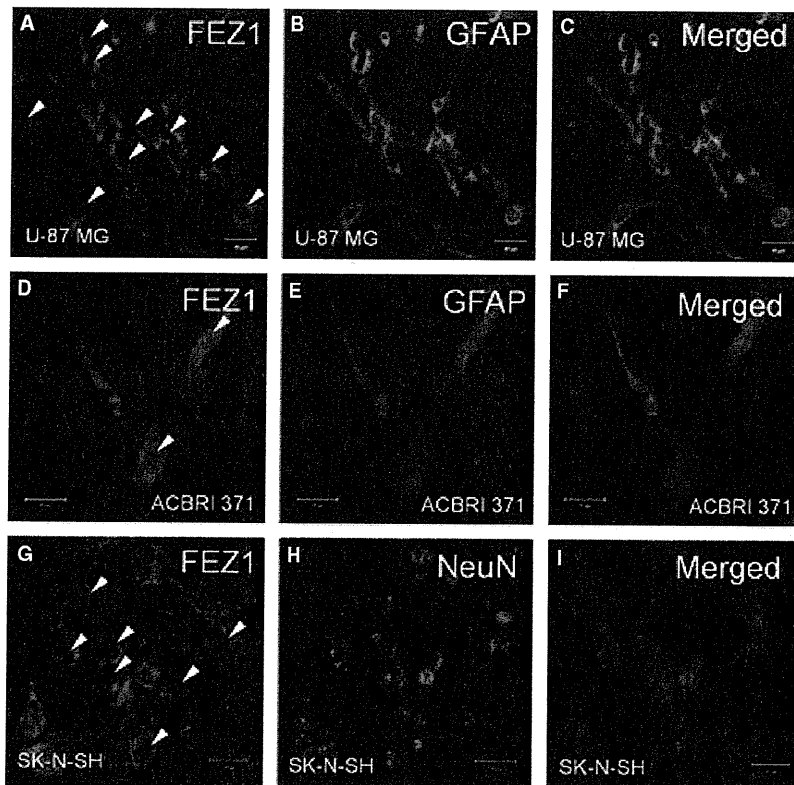
Fig. 4. Intracellular localization of fasciculation and elongation protein zeta 1 (FEZ1) protein in human astrocytic and neuronal cells. Figures A, B, and C show the intracellular localization of FEZ1 protein (A), glial fibrillary acidic protein (GFAP), an astrocyte marker (B), and the merged image showing the distribution of FEZ1 and GFAP (C) in the human astrocyte-derived cell line U-87 MG (scale bar: 40 μm). D, E, and F show the intracellular localization of FEZ1 protein (D), GFAP protein (E), and the merged image showing the distribution of FEZ1 and GFAP (F) in the human primary astrocyte cell culture ACBRI371 (scale bar: 40 μm). Figures G, H, and I show the intracellular localization of FEZ1 protein (G), the neuronal specific nuclear protein (NeuN) (H), and the merged image showing the distribution of FEZ1 and NeuN (I) in the human neuron-derived cell line SK-N-SH (scale bar: 20 μm). Cell nuclei were stained with 4',6-diamidino-2-phenylindole (DAPI, blue) (C, F, I). Arrow heads indicate nuclei of cells lacking FEZ1 signal.

concentrations did not alter FEZ1 protein expression levels in SK-N-SH cells (data not shown). Following treatment with the mood stabilizers at the high concentrations, only VPA increased the FEZ1 protein expression level in SK-N-SH cells (Fig. 3F).

Discussion

Among the four mood stabilizers, VPA affected the expression of the largest numbers of genes. VPA may exert its effect on transcriptional regulation by inhibiting histone deacetylase (HDAC) activity (33, 34); however, it remains uncertain whether the strong effect of VPA on transcriptional regulation is relevant to its mood-stabilizing effect and/or HDAC inhibition-mediated teratogenesis (35). It is interesting that LTG also affects a relatively large number of genes, despite the use of a concentration of LTG in the microarray experiments that was close to the lower limit of its therapeutic range (36, 37). LTG may have unknown mechanisms of

action that are relevant to its potent effect on transcriptional regulation.

The clustering analysis suggested that Li and VPA regulated the transcriptional activities of a common set of genes, whereas CBZ with LTG affected a different set of genes. Li and VPA have been reported to share common molecular mechanisms of action, including effects on glycogen synthase kinase 3β (38, 39) and phosphatidylinositol (40) signaling, which may underlie the common effects of Li and VPA on transcriptional regulation in U-87 MG cells. CBZ and LTG may share other unknown mechanisms which cause the observed transcriptional alterations in astrocytes.

Interestingly, only VPA increased FEZ1 protein expression in a neuron-derived cell line at a concentration representing the higher limit of the therapeutic range, while Li, CBZ, and LTG did not induce FEZ1 protein expression in neuronal cells at any concentration. The FEZ1 gene has been functionally characterized in the rodent brain and

495

a human neuron-derived cell line (41). These rodent studies have indicated that FEZ1 is preferentially expressed in neuronal cells and involved in normal axonal bundling, elongation within axon bundles of neurons, transport of intracellular components (including mitochondria), and release of neurotransmitters (32, 42, 43). FEZ1 protein is phosphorylated by PKCζ and then translocated from the cytoplasmic membrane to the cytoplasm, where it induces axonal growth and neuronal differentiation (44). FEZ1 protein has also been reported to localize to growth cones and associate with F-actin in SK-N-SH cells and cultured hippocampal neurons (41). Although the mechanism underlying its transcriptional regulation requires further investigation, induction of FEZ1 protein in neuronal cells by VPA might contribute to axonal bundling, transport of intracellular components, and neurotransmitter release.

The most intriguing finding of the genome-wide expression analysis of mood-stabilizer-treated U-87 MG cells was that only the FEZ1 and RBM14 transcripts were substantially induced and suppressed by all four mood stabilizers. The significant induction of FEZ1 molecules at both the transcript and the protein levels was verified by qRT-PCR and western blotting. Although FEZ1 transcript levels were significantly increased by the four mood stabilizers at lower concentrations, protein levels increased only at higher Li and CBZ concentrations. In general, changes in protein levels depend on levels of the transcript, translation efficiency, and degradation of the existing protein (45). Although the modest increase in FEZ1 transcripts after Li and CBZ treatments at lower concentrations may not be sufficient to yield a corresponding increase in FEZ1 translation, it implies that higher doses of Li and CBZ may increase transcript levels to a degree that allows for increased FEZ1 translation. Mood stabilizers might somehow affect translation efficiency and degradation of the existing protein as well, although these possibilities were not addressed in this study.

In addition to neuronal cells, FEZ1 is expressed in cultured rat neonatal astrocytes (46); however, it is expressed at barely detectable levels in adult astrocytes and oligodendrocytes (32). In our experiments, unlike the previous adult rodent studies, FEZ1 protein was expressed in the cytoplasm of both transformed and primary astrocytes, as well as in neuronal cells from the human adult brain, while it was not detectable in the human oligodendrocyte cell line (data not shown). No differences were detected in the intracellular distribution pattern of the FEZ1 protein between the human astrocytic and neuronal cells.

In general, the transcription of genes in certain cell types can vary among species. One example of this is the transcriptional regulation of toll-like receptors and nitric oxide synthase 2 in humans and rodents (47, 48). While exons 2-10 of human FEZ1 and rodent Fez1 are highly homologous (mouse: 90%, rat: 91%), exon 1 and the promoter region are not. This difference in the promoter region may underlie the expression of the gene in human astrocytes, but its absence in rodents.

Astrocytes are compact round cells in the early developmental stages, and subsequently, they project highly branched cellular processes that form connections with other cell types or with brain structures, similar to the extension of axons and dendrites observed in neurons. The localization of FEZ1 proteins suggests that FEZ1 may be involved in the extension and maintenance of astrocyte processes, mitochondrial functions, and the development and maintenance of structural formations in astrocytes; however, the function of FEZ1 protein in astrocytes requires further investigation.

Although there are reports that FEZ1 transcripts are decreased in postmortem brain tissue of patients with schizophrenia (49) and that FEZ1 and schizophrenia are modestly associated (50), neither postmortem brain studies nor genetic association studies targeting FEZ1 have been reported. However, indirect evidence from animal models and cell culture studies suggests the possible involvement of FEZ1 dysfunction in the pathogenesis of BD. To this end, FEZ1 knockout mice are hypersensitive to psychostimulant treatment (51), which suggests that hypofunction of FEZ1 may contribute to hyperdopaminergic conditions which have been implicated in the pathogenesis of the manic state of BD (52). In addition, FEZ1 has been reported to play an important role in the establishment of neuronal polarity by controlling the axonal transport of mitochondria (53, 54). Thus, an impairment of FEZ1 might be involved in the mitochondrial dysfunction implicated in BD (55, 56). Further studies will be needed to investigate abnormalities in FEZ1 expression and function in postmortem brains of BD subjects.

Our finding that four widely prescribed mood stabilizers commonly induced FEZ1 protein expression in astrocyte-derived cells raises the question of what the link is between the mechanisms of action of the mood stabilizers and FEZ1 induction. It is also unclear whether FEZ1 induction is specific to these mood stabilizers, and whether this induction is involved in the mood-stabilizing effects of these drugs. Further studies

will be needed to address these issues and the involvement of FEZ1 in the pathogenesis of BD.

Although the RBM14 transcript was suppressed by the mood stabilizer treatments, RBM14 protein expression was not affected by any of the mood stabilizers. While protein levels generally correlate with transcript levels, there can be discrepancies due to variability in translation efficiency and protein degradation (45). Thus, RBM14 translation efficiency may have increased or RBM14 degradation may have decreased in parallel with the decrease in RBM14 transcripts. Since RBM14 exerts its cellular effects by encoding the coactivator activator (CoAA) protein (57), the suppression of RBM14 transcripts may not be directly relevant to the mechanism of action of mood stabilizers. However, there remains the possibility that decreases in RBM14 transcripts may influence cellular function by modulating the expression of other transcripts.

Besides the genes commonly altered by the four mood stabilizers, each mood stabilizer uniquely altered the expression of certain genes with robust fold changes as shown in Tables 1 and 2. Although further studies will be needed to characterize the function of these regulated genes and their roles in mood stabilization, previous studies have suggested the possible involvement of some of these genes in the mechanism of action of the respective mood stabilizer. For example, VPA induced gamma-aminobutyric acid A receptor, beta 1 (GABRB1) and growth associated protein 43 (GAP43) transcripts by 330% and 328%, respectively (Table 1). GABA A receptor is expressed in both astrocytes and neurons. The GABA A receptor is thought to transfer signals from inhibitory interneurons to adjacent glial cells, and may regulate extracellular Cl⁻ concentrations in the vicinity of a GABAergic synapse (58). The SPECT study showed that levels of GABA A receptors were decreased in the sensory motor cortex of mood disorder patients with akinetic catatonia (59), whereas GABA receptors were increased in the rodent hippocampus after VPA treatment (60). These disease-related or VPA-induced alterations in GABA receptor expression may, at least in part, reflect the expression of GABA A receptors in astrocytes.

VPA was previously reported to increase neuronal GAP43 and cell survival *in vitro* (61). The present study demonstrated that VPA also induces GAP43 in astrocytes. Although GAP43 is a calmodulin-binding phosphoprotein primarily found in neuronal growth cones and is an intrinsic presynaptic determinant for neurite outgrowth and plasticity (62), it is also expressed in astrocytes, in particular type 2 astrocytes (63, 64). One study reported that ischemic injury induces GAP43 expression in reactive astrocytes, which protect the brain from ischemic injury by normalizing extracellular fluid H^+ or glutamate levels, or by releasing neuronal growth factors (65, 66). Given that postmortem brain studies have shown that GAP43 expression is significantly reduced in the anterior cingulate cortex of BD patients (67) and the prefrontal cortex of depressed suicide victims (68), VPA might exert its effects by inducing GAP43 levels.

DNA polymerase eta (POLH) increased by 60% after CBZ treatment, whereas interferon-induced transmembrane protein 3 (IFITM3) decreased by 37% after LTG treatment (Tables 1 and 2). Postmortem brain microarray analyses showed that POLH expression was decreased in the hippocampal CA1 region (69), and IFITM3 was increased in the prefrontal cortex of BD patients (70). This suggests the possibility that CBZ-induced POLH expression and LTG-mediated IFITM3 suppression may normalize the altered levels of these genes in affected brains. Thus, transcriptional regulation may underlie the mood-stabilizing actions of these drugs.

In conclusion, the microarray data obtained for human astrocytic cells identified FEZ1 as a gene that is commonly induced by the four mood stabilizers, Li, VPA, CBZ, and LTG. Unlike the studies performed in rodents, in the present study FEZ1 was expressed in the cytoplasm of human astrocytic cells and neuronal cells. Our data suggest that FEZ1 may play important roles in human astrocytes, and that mood stabilizers might exert their cytoprotective and mood-stabilizing effects via FEZ1 induction in astrocytes. Further studies will be needed to address the involvement of FEZ1 in the mechanisms of action of mood stabilizers and the pathogenesis of BD.

Acknowledgements

References

1. Williams R, Ryves WJ, Dalton EC et al. A molecular cell biology of lithium. Biochem Soc Trans 2004; 32: 799–802.

2. Di Daniel E, Cheng L, Maycox PR, Mudge AW. The common inositol-reversible effect of mood stabilizers on neurons does not involve GSK3 inhibition, myo-inositol-1-phosphate synthase or the sodium-dependent myo-inositol transporters. Mol Cell Neurosci 2006; 32: 27–36.

3. Beaulieu JM, Caron MG. Looking at lithium: molecular moods and complex behaviour. Mol Interv 2008; 8: 230–241.

4. O'Brien WT, Klein PS. Validating GSK3 as an in vivo target of lithium action. Biochem Soc Trans 2009; 37: 1133–1138.

5. Quiroz JA, Gould TD, Manji HK. Molecular effects of lithium. Mol Interv 2004; 4: 259–272.

6. Shaltiel G, Dalton EC, Belmaker RH, Harwood AJ, Agam G. Specificity of mood stabilizer action on neuronal growth cones. Bipolar Disord 2007; 9: 281–289.

7. Leng Y, Liang MH, Ren M, Marinova Z, Leeds P, Chuang DM. Synergistic neuroprotective effects of lithium and valproic acid or other histone deacetylase inhibitors in neurons: roles of glycogen synthase kinase-3 inhibition. J Neurosci 2008; 28: 2576–2588.

8. Du J, Gray NA, Falke C, Yuan P, Szabo S, Manji HK. Structurally dissimilar antimanic agents modulate synaptic plasticity by regulating AMPA glutamate receptor subunit GluR1 synaptic expression. Ann NY Acad Sci 2003; 1003: 378–380.

9. Friedrich MJ. Molecular studies probe bipolar disorder. JAMA 2005; 293: 535–536.

10. Doetsch F, Caillé I, Lim DA, García-Verdugo JM, Alvarez-Buylla A. Subventricular zone astrocytes are neural stem cells in the adult mammalian brain. Cell 1999; 97: 703–716.

11. Hama K, Arii T, Kosaka T. Three-dimensional organization of neuronal and glial processes: high voltage electron microscopy. Microsc Res Tech 1994; 29: 357–367.

12. Haydon PG. GLIA: listening and talking to the synapse. Nat Rev Neurosci 2001; 2: 185–193.

13. Kosaka T, Hama K. Three-dimensional structure of astrocytes in the rat dentate gyrus. J Comp Neurol 1986; 249: 242–260.

14. Ventura R, Harris KM. Three-dimensional relationships between hippocampal synapses and astrocytes. J Neurosci 1999; 19: 6897–6906.

15. Rajkowska G. Cell pathology in bipolar disorder. Bipolar Disord 2002; 4: 105–116.

16. Ongür D, Drevets WC, Price JL. Glial reduction in the subgenual prefrontal cortex in mood disorders. Proc Natl Acad Sci USA 1998; 95: 13290–13295.

17. Rajkowska G, Halaris A, Selemon LD. Reductions in neuronal and glial density characterize the dorsolateral prefrontal cortex in bipolar disorder. Biol Psychiatry 2001; 49: 741–752.

18. Manji HK, Moore GJ, Rajkowska G, Chen G. Neuroplasticity and cellular resilience in mood disorders. Mol Psychiatry 2000; 5: 578–593.

19. Webster MJ, O'Grady J, Kleinman JE, Weickert CS. Glial fibrillary acidic protein mRNA levels in the cingulate cortex of individuals with depression, bipolar disorder and schizophrenia. Neuroscience 2005; 133: 453–461.

20. Johnston-Wilson NL, Sims CD, Hofmann JP et al. Disease-specific alterations in frontal cortex brain proteins in schizophrenia, bipolar disorder, and major depressive disorder. The Stanley Neuropathology Consortium. Mol Psychiatry 2000; 5: 142–149.

21. Andreazza AC, Cassini C, Rosa AR et al. Serum S100B and antioxidant enzymes in bipolar patients. J Psychiatr Res 2007; 41: 523–529.

22. Roche S, Cassidy F, Zhao C et al. Candidate gene analysis of 21q22: support for S100B as a susceptibility gene for bipolar affective disorder with psychosis. Am J Med Genet B Neuropsychiatr Genet 2007; 144B: 1094–1096.

23. Pardo R, Andreolotti AG, Ramos B, Picatoste F, Claro E. Opposed effects of lithium on the MEK-ERK pathway in neural cells: inhibition in astrocytes and stimulation in neurons by GSK3 independent mechanisms. J Neurochem 2003; 87: 417–426.

24. Chen PS, Peng GS, Li G et al. Valproate protects dopaminergic neurons in midbrain neuron/glia cultures by stimulating the release of neurotrophic factors from astrocytes. Mol Psychiatry 2006; 11: 1116–1125.

25. Lubrich B, van Calker D. Inhibition of the high affinity myo-inositol transport system: a common mechanism of action of antibipolar drugs? Neuropsychopharmacology 1999; 21: 519–529.

26. Li B, Zhang S, Li M, Zhang H, Hertz L, Peng L. Down-regulation of GluK2 kainate receptor expression by chronic treatment with mood-stabilizing anti-convulsants or lithium in cultured astrocytes and brain, but not in neurons. Neuropharmacology 2009; 57: 375–385.

27. Li B, Zhang S, Li M, Hertz L, Peng L. Chronic treatment of astrocytes with therapeutically relevant fluoxetine concentrations enhances cPLA2 expression secondary to 5-HT2B-induced, transactivation-mediated ERK1/2 phosphorylation. Psychopharmacology 2009; 207: 1–12.

28. Song D, Du T, Li B et al. Astrocytic alkalinization by therapeutically relevant lithium concentrations: implications for myo-inositol depletion. Psychopharmacology 2008; 200: 187–195.

29. Dahlquist KD, Salomonis N, Vranizan K, Lawlor SC, Conklin BR. GenMAPP, a new tool for viewing and analyzing microarray data on biological pathways. Nat Genet 2002; 31: 19–20.

30. Miller LD, Long PM, Wong L, Mukherjee S, McShane LM, Liu ET. Optimal gene expression analysis by microarrays. Cancer Cell 2002; 2: 353–361.

31. Choe SE, Boutros M, Michelson AM, Church GM, Halfon MS. Preferred analysis methods for Affymetrix GeneChips revealed by a wholly defined control dataset. Genome Biol 2005; 6: R16.

32. Honda A, Miyoshi K, Baba K et al. Expression of fasciculation and elongation protein zeta-1 (FEZ1) in the developing rat brain. Brain Res Mol Brain Res 2004; 122: 89–92.

33. Busa WB, Gimlich RL. Lithium-induced teratogenesis in frog embryos prevented by a polyphosphoinositide cycle intermediate or a diacylglycerol analog. Dev Biol 1989; 132: 315–324.

34. Phiel CJ, Zhang F, Huang EY, Guenther MG, Lazar MA, Klein PS. Histone deacetylase is a direct target of valproic acid, a potent anticonvulsant, mood stabilizer, and teratogen. J Biol Chem 2001; 276: 36734–36741.

35. Gurvich N, Berman MG, Wittner BS, Gentleman RC, Klein PS, Green JB. Association of valproate-induced teratogenesis with histone deacetylase inhibition in vivo. FASEB J 2005; 19: 1166–1168.

36. May TW, Rambeck B, Jurgens U. Serum concentrations of lamotrigine in epileptic patients: the influence of dose and comedication. Ther Drug Monit 1996; 18: 523–531.

37. Fraser AD, MacNeil W, Isner AF, Camfield PR. Lamotrigine analysis in serum by high-performance liquid chromatography. Ther Drug Monit 1995; 17: 174–178.

38. Chen G, Huang LD, Jiang YM, Manji HK. The mood-stabilizing agent valproate inhibits the activity of glycogen synthase kinase-3. J Neurochem 1999; 72: 1327–1330.

39. De Sarno P, Li X, Jope RS. Regulation of Akt and glycogen synthase kinase-3 beta phosphorylation by sodium valproate and lithium. Neuropharmacology 2002; 43: 1158–1164.

40. Williams RS, Cheng L, Mudge AW, Harwood AJ. A common mechanism of action for three mood-stabilizing drugs. Nature 2002; 417: 292–295.

41. Miyoshi K, Honda A, Baba K et al. Disrupted-In-Schizophrenia 1, a candidate gene for schizophrenia, participates in neurite outgrowth. Mol Psychiatry 2003; 8: 685–694.

42. Bloom L, Horvitz HR. The Caenorhabditis elegans gene unc-76 and its human homologs define a new gene family involved in axonal outgrowth and fasciculation. Proc Natl Acad Sci USA 1997; 94: 3414–3419.

43. Assmann EM, Alborghetti MR, Camargo ME, Kobarg J. FEZ1 dimerization and interaction with transcription regulatory proteins involves its coiled-coil region. J Biol Chem 2006; 281: 9869–9881.

44. Kuroda S, Nakagawa N, Tokunaga C, Tatematsu K, Tanizawa K. Mammalian homologue of the Caenorhabditis elegans UNC-76 protein involved in axonal outgrowth is a protein kinase C zeta-interacting protein. J Cell Biol 1999; 144: 403–411.

45. de Sousa Abreu R, Penalva LO, Marcotte EM, Vogel C. Global signatures of protein and mRNA expression levels. Mol Biosyst 2009; 5: 1512–1526.

46. He J, Liu J, Zhang Z, Sun M, Zhu T, Xia C. Expression of fasciculation and elongation protein zeta-1 (FEZ1) in cultured rat neonatal astrocytes. Mol Cell Biochem 2009; 325: 159–167.

47. Rehli M. Of mice and men: species variations of Toll-like receptor expression. Trends Immunol 2002; 23: 375–378.

48. Rico D, Vaquerizas JM, Dopazo H, Bosca L. Identification of conserved domains in the promoter regions of nitric oxide synthase 2: implications for the species-specific transcription and evolutionary differences. BMC Genomics 2007; 8: 271.

49. Lipska BK, Peters T, Hyde TM et al. Expression of DISC1 binding partners is reduced in schizophrenia and associated with DISC1 SNPs. Hum Mol Genet 2006; 15: 1245–1258.

50. Yamada K, Nakamura K, Minabe Y et al. Association analysis of FEZ1 variants with schizophrenia in Japanese cohorts. Biol Psychiatry 2004; 56: 683–690.

51. Sakae N, Yamasaki N, Kitaichi K et al. Mice lacking the schizophrenia-associated protein FEZ1 manifest hyperactivity and enhanced responsiveness to psychostimulants. Hum Mol Genet 2008; 17: 3191–3203.

52. Cousins DA, Butts K, Young AH. The role of dopamine in bipolar disorder. Bipolar Disord 2009; 11: 787–806.

53. Fujita T, Maturana AD, Ikuta J et al. Axonal guidance protein FEZ1 associates with tubulin and kinesin motor protein to transport mitochondria in neurites of NGF-stimulated PC12 cells. Biochem Biophys Res Commun 2007; 361: 605–610.

54. Ikuta J, Maturana A, Fujita T et al. Fasciculation and elongation protein zeta-1 (FEZ1) participates in the polarization of hippocampal neuron by controlling the mitochondrial motility. Biochem Biophys Res Commun 2007; 353: 127–132.

55. Kato T. The role of mitochondrial dysfunction in bipolar disorder. Drug News Perspect 2006; 19: 597–602.

56. Quiroz JA, Gray NA, Kato T, Manji HK. Mitochondrially mediated plasticity in the pathophysiology and treatment of bipolar disorder. Neuropsychopharmacology 2008; 33: 2551–2565.

57. Auboeuf D, Dowhan DH, Li X et al. CoAA, a nuclear receptor coactivator protein at the interface of transcriptional coactivation and RNA splicing. Mol Cell Biol 2004; 24: 442–453.

58. MacVicar BA, Tse FW, Crichton SA, Kettenmann H. GABA-activated Cl- channels in astrocytes of hippocampal slices. J Neurosci 1989; 9: 3577–3583.

59. Northoff G, Steinke R, Czcervenka C et al. Decreased density of GABA-A receptors in the left sensorimotor cortex in akinetic catatonia: investigation of in vivo benzodiazepine receptor binding. J Neurol Neurosurg Psychiatry 1999; 67: 445–450.

60. Motohashi N. GABA receptor alterations after chronic lithium administration. Comparison with carbamazepine and sodium valproate. Prog Neuropsychopharmacol Biol Psychiatry 1992; 16: 571–579.

61. Yuan PX, Huang LD, Jiang YM, Gutkind JS, Manji HK, Chen G. The mood stabilizer valproic acid activates mitogen-activated protein kinases and promotes neurite growth. J Biol Chem 2001; 276: 31674–31683.

62. Aigner L, Arber S, Kapfhammer JP et al. Overexpression of the neural growth-associated protein GAP-43 induces nerve sprouting in the adult nervous system of transgenic mice. Cell 1995; 83: 269–278.

63. da Cunha A, Vitković L. Regulation of immunoreactive GAP-43 expression in rat cortical macroglia is cell type specific. J Cell Biol 1990; 111: 209–215.

64. Vitković L, Steisslinger HW, Aloyo VJ, Mersel M. The 43-kDa neuronal growth-associated protein (GAP-43) is present in plasma membranes of rat astrocytes. Proc Natl Acad Sci USA 1988; 85: 8296–8300.

65. Yamada K, Goto S, Oyama T, Inoue N, Nagahiro S, Ushio Y. In vivo induction of the growth associated protein GAP43/B-50 in rat astrocytes following transient middle cerebral artery occlusion. Acta Neuropathol 1994; 88: 553–557.

66. Petito CK, Chung M, Halaby IA, Cooper AJ. Influence of the neuronal environment on the pattern of reactive astrocytosis following cerebral ischemia. Prog Brain Res 1992; 94: 381–387.

67. Eastwood SL, Harrison PJ. Synaptic pathology in the anterior cingulate cortex in schizophrenia and mood disorders. A review and a Western blot study of synaptophysin, GAP-43 and the complexins. Brain Res Bull 2001; 55: 569–578.

68. Hrdina P, Faludi G, Li Q et al. Growth-associated protein (GAP-43), its mRNA, and protein kinase C (PKC) isoenzymes in brain regions of depressed suicides. Mol Psychiatry 1998; 3: 411–418.

69. Benes FM, Lim B, Subburaju S. Site-specific regulation of cell cycle and DNA repair in post-mitotic GABA cells in schizophrenic versus bipolars. Proc Natl Acad Sci USA 2009; 106: 11731–11736.

70. Iwamoto K, Kakiuchi C, Bundo M, Ikeda K, Kato T. Molecular characterization of bipolar disorder by comparing gene expression profiles of postmortem brains of major mental disorders. Mol Psychiatry 2004; 9: 406–416.

A De Novo Deletion of 20q11.2–q12 in a Boy Presenting With Abnormal Hands and Feet, Retinal Dysplasia, and Intractable Feeding Difficulty

Yoko Hiraki,[1,2] Akira Nishimura,[2] Michiko Hayashidani,[3] Yoshiko Terada,[4] Gen Nishimura,[5] Nobuhiko Okamoto,[6] Sachiko Nishina,[7] Yoshinori Tsurusaki,[2] Hiroshi Doi,[2] Hirotomo Saitsu,[2] Noriko Miyake,[2] and Naomichi Matsumoto[2]*

[1]Hiroshima Municipal Center for Child Health and Development, Hiroshima, Japan

[2]Department of Human Genetics, Yokohama City University Graduate School of Medicine, Yokohama, Japan

[3]Medical Center for Premature and Neonatal Infants, Hiroshima City Hospital, Hiroshima, Japan

[4]Department of Ophthalmology, Hiroshima City Hospital, Hiroshima, Japan

[5]Department of Pediatric Imaging, Tokyo Metropolitan Children's Medical Center, Tokyo, Japan

[6]Department of Medical Genetics, Osaka Medical Center and Research Institute for Maternal and Child Health, Osaka, Japan

[7]Department of Ophthalmology, National Center for Child Health and Development, Tokyo, Japan

Proximal interstitial deletions involving 20q11–q12 are very rare. Only two cases have been reported. We describe another patient with 20q11.21–q12 deletion. We precisely mapped the 6.5-Mb deletion and successfully determined the deletion landmarks at the nucleotide level. Common clinical features among the three cases include developmental delay, intractable feeding difficulties with gastroesophageal reflux, and facial dysmorphism including triangular face, hypertelorism, and hypoplastic alae nasi, indicating that the 20q11.2–q12 deletion can be a clinically recognizable syndrome. This is also supported by the fact that the three deletions overlap significantly. In addition, unique features such as arthrogryposis/fetal akinesia (hypokinesia) deformation and retinal dysplasia are recognized in the patient reported herein. © 2011 Wiley-Liss, Inc.

How to Cite this Article:
Hiraki Y, Nishimura A, Hayashidani M, Terada Y, Nishimura G, Okamoto N, Nishina S, Tsurusaki Y, Doi H, Saitsu H, Miyake N, Matsumoto N. 2011. A de novo deletion of 20q11.2–q12 in a boy presenting with abnormal hands and feet, retinal dysplasia, and intractable feeding difficulty.

Am J Med Genet Part A 155:409–414.

at 20q11.21–q12, clinically showing mental retardation, minor craniofacial anomalies, and intractable feeding difficulties. The deletion has been precisely analyzed at the nucleotide level and his detailed clinical manifestations will be presented.

INTRODUCTION

Interstitial deletions of the long arm of chromosome 20 are rare. To our knowledge, a total of 12 patients have been reported in the literature [Petersen et al., 1987; Shabtai et al., 1993; Aldred et al., 2002; Genevieve et al., 2005; Callier et al., 2006; Borozdin et al., 2007; Iqbal and Al-Owain, 2007]. Among them, only two cases showed the proximal q deletion (20q11–q12), not extending to q13 [Callier et al., 2006; Iqbal and Al-Owain, 2007]. One patient had a 6.6-Mb deletion at 20q11.21–q11.23 [Callier et al., 2006], and the other [Iqbal and Al-Owain, 2007] showed a 6.8-Mb deletion at 20q11.2–q12. Here, we report on the third patient with a 6.5-Mb deletion

CLINICAL REPORT

The 18-month-old boy was the first product of healthy 22-year-old mother and 25-year-old father without any consanguinity. Pregnancy was uneventful. Family history was unremarkable. He was born by spontaneous vaginal delivery at 38 weeks of gestation. Birth weight was 2,230 g (−1.7 SD), length 44.0 cm (−1.9 SD), and OFC 32.5 cm (−0.3 SD). Multiple malformations including patent ductus arteriosus, patency of foramen ovale, and dysmorphic face were noted. He was tube-fed due to poor swallowing and oxygen therapy was required until 4 months because of respiratory disturbance. X-ray examination at age of 1 month revealed small thorax and mild slender long bones. In addition, right eye retinal fold was pointed out. At age of 3 months, upper gastrointestinal tract was investigated because of recurrent vomiting, and gastroesophageal reflux (GER) and esophageal hiatus hernia were found. Esophageal hiatus hernia was alleviated spontaneously, but GER persisted.

At age of 4 months, he was referred to us for evaluation of his developmental delay. He was noted to have the following craniofacial features: triangular face, premature closure fontanelle, slopping forehead, wide bending eyebrows, hypertelorism, low-set and posterior rotated ears, long columella nasi, mild hypoplastic alae nasi, short and well-defined philtrum, thin lips with tucked-in lower lip, submucosal cleft palate, microretrognathia and posterior low hair-line (Fig. 1A,B and Table I). Additionally, abnormal hands and feet were recognized, consisted of restriction of all proximal interphalangeal joints and over-extension of all distal interphalangeal joints of hands and feet, radial deviation of 2nd fingers, clinodactyly of the 2nd and 5th fingers, lack of flexion creases bilaterally, right preaxial polydactyly, left single palmar, and talipes valgus. Mild restriction of elbow, hip and knee joints bilaterally was also noted (Fig. 1C–E and Table I).

At 15 months, his weight was 7.5 kg (−2.3 SD), length 71.8 cm (−2.7 SD), and OFC 44.4 cm (−1.6 SD). He could roll over one side and shift a toy from one hand to the other. Social smile was seen, but he could not recognize his parents (DQ 48). His dysphagia persisted based on the modified swallowing study [Kanda et al., 2005]; he required tube-feeding, and rejected oral intake. Ophthalmic examination at 15 months revealed broom-like pattern of retinal vessels extending from optic disc to periphery with a falciform retinal fold in the right eye, causing visual impairment. In the left eye, mild opacity in the lateral portion of vitreous body was found. These findings led to the diagnosis of bilateral retinal dysplasia. Anterior segment and optic disc were normal. Left hearing loss was suspected by auditory brainstem response, otoacoustic emission, and behavioral observation audiometry. Brain magnetic resonance imaging revealed cortical atrophy and mild ventriculomegaly. Blood biochemistry and abdominal ultrasonographic examination were all normal. Serological TORCH (toxoplasma, rubella, cytomegarovirus, and herpes simplex) testing was negative. At 18 months, the shortening of 5th middle phalanges of fingers and absence of middle phalanges of the toes were confirmed by X-ray examination.

CYTOGENETIC AND MOLECULAR ANALYSIS

G-banded chromosomal analysis (550 bands level) of the patient's blood lymphocytes indicated normal karyptype (46,XY) (data not shown). Fluorescence in situ hybridization (FISH) analysis using all
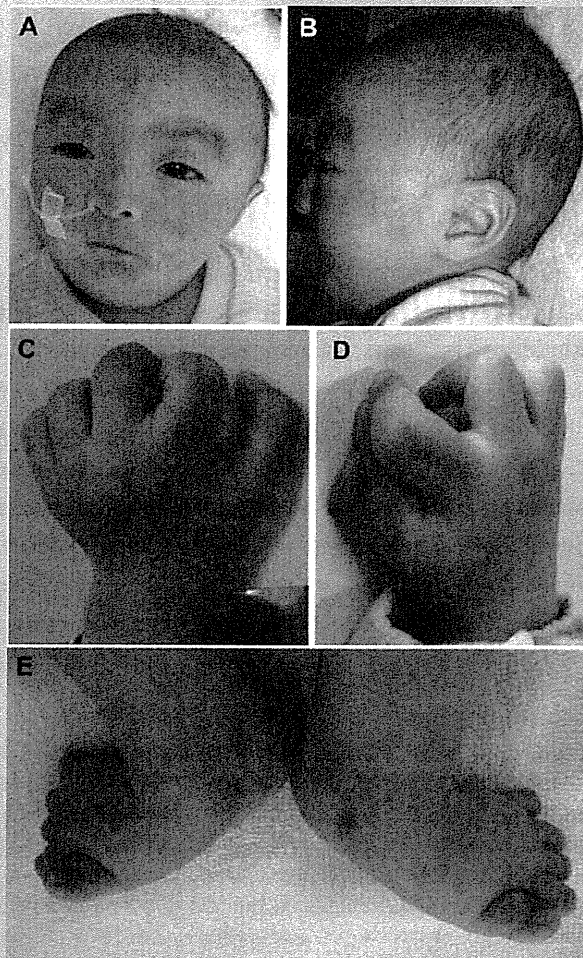

FIG. 1. Photographs of the patient at age of 4 months. A,B: Facial abnormalities including triangular face, wide and bending eyebrows, hypertelorism, long columella, thin lips with tucked-in lower lip, and microretrognathia were recognized. C (left hand) and D (right): Bilateral camptodactyly associated with radial deviation of the 2nd fingers and clinodactyly of the 2nd and 5th, and right preaxial polydactyly were noted. E: Camptodactyly with talipes valgus in both feet.

chromosomal subtelomeric clones did not show any abnormalities. Array CGH analysis using NimbleGen 385K Array (Roche NimbleGen, Inc., Madison, WI) demonstrated a 6.5-Mb heterozygous deletion at 20q11.2–q12 (UCSC genome coordinates 2006 Mar. version, chromosome 20: 31,269,661–37,782,841 bp) (Fig. 2A). The deletion was also confirmed by FISH using BACs (RP11-322B6 and RP11-782C16 at 21q11.21, and RP11-54P22 and RP11-467J15 at 20q12), RP11-787C16 and RP11-54P22 was deleted while RP11-322B6 and RP11-467J15 were not deleted (Fig. 3). The deletion junction was successfully amplified by PCR using primers (Primer A: 5′-TGA TAG AGC CAA CTG GGT CAT GTG C-3′, Primer C: 5′-TCT AGC TTG CTG AAT TCC TGC CTG A-3′) (Fig. 2B) and its product was sequenced. The deleted region was from 31,274,015 to 37,783,826 bp (6,509,811 bp) with 5-bp overlap (ATAGA) (Fig. 2C). The deletion occured de novo as FISH and